Structure and dielectric properties of potassium niobate nano glass-ceramics

Reenamoni Saikia Chaliha, V. S. Tiwari[a], P. K. Gupta[a], K. Annapurna, Anal Tarafder, Basudeb Karmakar[*]

Glass Technology Laboratory, Central Glass and Ceramic Research Institute (Council of Scientific and Industrial Research) 196, Raja S.C. Mullick Road, Kolkata 700032, India

[a]Laser Materials Development and Devices Division, Raja Ramanna Center for Advanced Technology, Indore 452 013, India

Abstract

Glasses in the composition of $25K_2O$-$25Nb_2O_5$-$50SiO_2$ (mol %) doped with Eu_2O_3 (0.5 wt% in excess) have been prepared by melt quenching technique and nano-ceramized isothermally at 800°C for different duration. The formed nanocrystalline $KNbO_3$ phase, crystallite size and morphology are examined by X-ray diffraction, Fourier transform infrared reflection spectroscopy, field emission scanning and transmission electron microscopes. The frequency and temperature dependent dielectric constant and loss tangent are measured in the frequency and temperature ranges 0.1–1000 kHz and 200-500°C respectively. The dielectric constant and loss tangent are found to decrease with increasing frequency and increase with increasing temperature. The dielectric constant and loss tangent versus temperature curve at different frequency revealed the phase transition of $KNbO_3$ from paraelectric cubic to ferroelectric tetragonal around 425º and 397ºC (Curie temperature) for nano glass-ceramics obtained after 1 and 200 h ceramming respectively.

Keywords: A. Nanostructures, C. X-ray diffraction, C. Infrared spectroscopy, D. Dielectric properties, D. Ferroelectricity

[*]Corresponding author. Tel.: +91-33 2473 3469; fax: +91-33 2473 0957
E-mail address: basudebk@cgcri.res.in (B. Karmakar)

1. Introduction

Ferroelectric potassium niobate ($KNbO_3$) with ABO_3-type perovskite crystal structure is characterized by large electro-optic coefficient, non linear optical coefficient, excellent photorefractive properties and moderate dielectric constant [1]. It has attracted much attention because of its many applications in photonic and opto-electronic devices such as frequency doubling, tunable wave guiding, active laser host, holographic storage and surface acoustic wave [2-3]. Recently, potassium niobate ceramics were revisited in the interest of a search for environmental friendly lead-free piezoelectric materials [4]. Ferroelectric $KNbO_3$ exhibits three successive phase transitions similar to that of $BaTiO_3$ [5]. It shows structural phase transitions at -10ºC (rhombohedral to orthorhombic), 225ºC (orthorhombic to tetragonal) and 420ºC (tetragonal to cubic) [6]. Studies on dielectric properties of pure and doped $KNbO_3$ crystals and ceramics with variation of temperature have been reported [7-8]. As we aware, there is no report on variation of dielectric properties of $KNbO_3$ containing nano glass-ceramics. There has been an increasing interest in crystallized glasses containing $KNbO_3$ ferroelectric as an active crystalline phase because of cheaper and high-speed fabrication process of glass technology, in comparison to single crystal. Recently, we have reported the fluorescent properties of Eu^{3+}: $KNbO_3$ glass-ceramic nanocomposites [9].

In this paper, we address our investigation on the change of dielectric properties including phase transformation as a function of various frequencies and temperatures of Eu_2O_3 doped $KNbO_3$ glass-ceramic nanocomposites obtained under isothermal crystallization in the K_2O-Nb_2O_5-SiO_2 glass system. In addition to these, the process of crystallization has been studied by differential thermal analysis (DTA), X-ray diffraction

(XRD), Fourier transform infrared reflection spectroscopy (FTIRRS), field emission scanning electron microscopy (FESEM) and transmission electron microscopy (TEM).

2. Experimental procedure

The glass in the chemical composition of $25K_2O$-$25Nb_2O_5$-$50SiO_2$ (mol %) doped with 0.5 wt% Eu_2O_3 (in excess) was prepared using high purity K_2CO_3 (GR, 99.9%, Loba Chemie), Nb_2O_5 (GR, 99.9%, Loba Chemie), SiO_2 (99.99%) and Eu_2O_3 (99.9%, Alfa Aesar) by melting the well mixed chemical batch for 300 g glass in a platinum crucible at 1550°C for 2h. The melt was homogenized with an intermittent stirring and later it was quenched by pouring onto a pre-heated iron mould. The obtained glass block was subsequently annealed at 600°C for 1h in order to remove the internal stresses. The as-prepared glass block was cut into desired dimensions and optically polished for undertaking different experiments and measurements.

The DTA curve of powdered glass was recorded on a Netzsch STA 409 C/CD instrument from the room temperature to 1000°C at a heating rate of 10° C/min. The polished samples were heat-treated (ceramized) at 800°C for 0, 1 and 200 h after nucleating at 720°C temperature for 2 h. The XRD pattern was recorded using a Xpert-Pro diffractometer (CuKα) with nickel filtered and anchor scan parameters wavelength of 1.54060 Å at 25°C having the source power of 40 kV and 30 mA to identify the possible phases. The FTIR reflectance spectra of glass and glass-ceramics were recorded using a Perkin Elmer FTIRR spectrometer (Model 1615) in the wavenumber range 400-1500 cm^{-1} with a spectral resolution of $\pm$ 2 cm^{-1} and at a 15° angle of incidence after 16 scans.

The nanocrystallinity of the heat-treated glasses was examined by both FESEM and TEM. A Carl Zeiss high resolution Field Emission Electron Microscope (FESEM), model SUPRA 35 VP detector (lithium doped silicon) with the parameters Gun vacuum = 3×10^{-10} mbar, System vacuum = 2.65×10^{-5} mbar, Extractor current = 159.3 μA for FESEM measurement. Freshly fractured surfaces of the heat-treated glasses were etched in 1% HF aqueous solution for 60 s and were coated with a thin carbon film for the above measurements. The TEM of powdered samples was done on FEI (Technai 30ST) instrument.

Rectangular samples of 10 x 8 x 1 mm^3 size were coated with gold by sputtering technique and subjected to weak field dielectric measurements using HP4194A impedance analyzer. The dielectric constant and loss tangent were measured at various frequencies between 0.1–1000 kHz in the temperature range of 200-500°C. A programmable temperature controller (Eurotherm 902) was used to display and control the sample temperature with a heating/cooling rate of 2^oC/min. The temperature measurement was carried out with an accuracy of $\pm0.1^oC$ using a chrome-alumel thermocouple. All the dielectric data were recorded during cooling cycle.

3. Results and discussion

3.1 Physical and thermal properties

The prepared glass and heat-treated samples were transparent with tints of yellow. The recorded DTA curve of the powdered glass sample is shown in Fig. 1, which exhibited an inflection in the temperature range 650-730°C followed by two exothermic peaks at 763°C (T_{p1}) and 945°C (T_{p2}) corresponding to the potassium niobate ($KNbO_3$)

and potassium niobosilicate ($KNbSi_2O_7$) phase crystallization respectively. The glass transition temperature (T_g) estimated from the DTA curve is 676°C. From the DTA data, the glass thermal stability factor ($\Delta = T_{p1} - T_g$) has been determined and found to be 87°C. The reasonably high glass stability factor specifies the ability of this glass in forming nano-structured glass-ceramic under controlled heat-treatment. The first exothermal peak in the DTA thermogram can be attributed to the growth of $KNbO_3$ crystallites from nuclei in the glass bulk as well.

3.2 XRD analysis

The X-ray diffractograms of as-prepared glass along with the glass ceramic samples are depicted in Fig. 2. The XRD pattern of the as-prepared glass consists of only a broad hump around diffraction angle $2\theta = 29°$ indicating its amorphous nature. The structuring of this hump takes place in the XRD pattern of the heat treated glass ceramic samples along with the appearance of other well defined peaks around 15°, 16°, 25°, 29°, and 51° diffraction angles (2θ), which confirms the appearance of crystalline phase in the amorphous matrix. The diffraction pattern of glass-ceramics to some extent resembles known potassium niobate crystal phase JCPDS card file No. : 32-821. From the full width at half maximum (FWHM) values of the intense diffraction peak detected in the traces of the heat-treated samples of Fig. 2, the average crystallite sizes (diameter, d) were calculated by conventional procedure using the Scherrer's formula [10]

$$d = 0.9\lambda/\beta \cos\theta \qquad (1)$$

where, λ is the wavelength of X-ray radiation (CuKα = 1.5406Å), β is the full width at half maximum (FWHM) of the peak at 2θ. The diffraction peak located at $2\theta = 29°$ has

been considered for this estimation. The calculated average crystallite sizes are 6 and 12 nm for 1 and 200 h heat-treated samples respectively.

3.3 Fourier transform infrared reflectance spectroscopy

The FTIR reflectance spectra of the as-prepared and heat-treated samples in the wavenumber range 400-1500 cm^{-1} are shown in Fig. 3. From this figure, it is seen that the FTIRR spectrum of the as-prepared glass exhibits a broad reflection band centered at 933 cm^{-1} as a result of wider distribution of silicon structural units. This is an indication of the structural disorder existing in the amorphous network with the presence of SiO_4 tetrahedra and NbO_6 octahedra having different number of non-bridging oxygens, which is attributed to overlapping of Si-O and Nb-O stretching vibrations. In spite of the transparent nature of the heat-treated samples, their FTIR reflectance spectra reveal narrowing of the main reflection band with additional features arising at 1115, 748 and 400-600 cm^{-1} in comparison to the as prepared glass [11].

Considering the stronger force constant of the Si-O bonds than that of Nb-O ones, the reflection bands can be assigned in the FTIR reflectance spectra [12]. In the FTIRR spectra, the stretching modes of the Si-O-Si bonds of the SiO_4 tetrahedra with nonbridging oxygen (NBO) atoms are active in 1000-1100 cm^{-1} range and the stretching modes of the Nb-O bonds in the NbO_6 octahedra occur in the 700-800 cm^{-1} range.

According to the literature reports, in alkali niobium silicate glasses, NbO_6 with octahedra Nb-O bonds present as a lattice former in the Si-O bonds containing SiO_4 tetrahedral network. The alkali ions (K^+) play the role of charge compensators of excess negative charge at Nb^{5+} cations [13, 14]. In the present study, the observed systematic

variation of the FTIRR spectra of the as-prepared glass from that of the heat-treated glasses reveals the structural modifications occurring in the glass matrix as a result of the heat-treatment. Hence, it can be indicated that the heat-treatment changes the composition of the glassy matrix by forming two phases: the one, in the higher wavenumber side enriched of SiO_4 tetrahedra with *n* bridging oxygen atoms; the other, in the lower wavenumber side mainly containing less-distorted NbO_6 octahedra with no nonbridging oxygens. In order to maintain neutral charge condition, the latter phase contains a higher amount of K^+ ions as the NbO_6 octahedra are negatively charged. Hence, the rearrangement of the glassy matrix is an indicative of the fact that the alkali enriched phase begins to crystallize producing a nanostructure with the heat-treatment. The reflection bands around 1075 - 1130 cm^{-1} are associated with the ν_3 antisymmetric stretching vibration modes of the SiO_4 tetrahedra. The symmetric stretching mode ν_1 is assigned for the reflection bands lying in the range 840-970 cm^{-1} wavenumber. The reflection band at 1115 and 930 cm^{-1} wavenumber can be related to the asymmetric and symmetric stretching vibration modes of Si-O bonds in SiO_4 tetrahedra respectively, while the one at 748 cm^{-1} is due to the Nb-O stretching modes of distorted NbO_6 octahedra [15, 16]. Hence, it is revealed that in a phase separated matrix of the heat-treated samples, the crystallization starts at the interface between the two phases originating a redistribution of both types of structural units such as NbO_6 octahedra and SiO_4 tetrahedra. This corroborates that the reflection band centered at 748 cm^{-1} wavenumber is assigned as $KNbO_3$ crystal formation. The intensity of this reflection band increases with increase of heat-treatment time very slowly indicating that the further growth of $KNbO_3$ nanocrystallites at the interface is prevented for longer heat-treatment

times to satisfy the chemical composition required by the crystallizing phase [12]. Finally, all FTIRR spectra in Fig. 3 exhibit a band around 598 cm^{-1}, which is assigned to ν_2 bending vibration mode of the Si-O bond in the SiO_4 tetrahedron. Thus from the investigations carried out on the measured FTIR reflectance spectra of potassium niobium silicate glass and glass-ceramics as described above provide the information of crystallization with initial phase separation followed by advancement of $KNbO_3$ crystal formation in the glass matrix.

3.4 FESEM and TEM image analysis

The morphology and crystallite size in glass-ceramic samples have been examined by FESEM and TEM image analysis. Figs. 4 (a, b) present the FESEM micrograph of the sample heat-treated at 800°C for 1 and 200 h duration respectively. From the FESEM micrographs, it is clearly observed that the glassy matrix of the heat-treated samples initially phase separated on nanometric scale followed by incipient precipitation of defined crystallites within the Nb – K rich phase regions on the prolonged heat-treatments. The droplets have irregular shape and are spread out uniformly thought out the bulk glass matrix (volume crystallization). The size of the droplets was estimated to be about 20-40 nm. The TEM and HRTEM images of the sample heat treated for 1 and 200 h have been presented in Figs 5 (a, b, c, d) respectively. From these figures, precipitated crystallites and their atomic or lattice fringes are clearly observed. A comparison of the FESEM and TEM micrographs with the XRD data gives rise to another interesting result. The size of the crystallites estimated from the XRD patterns and TEM (6-12 nm) are lesser than the droplets observed in FESEM (20-40 nm),

suggesting that the crystallization starts at the interface between the droplets and the matrix followed by the growth of the crystallites inside these droplets. Because of these phenomena, there is a change of the matrix composition, which prevents the further growth of the crystallites, regardless of the increase in the heat-treatment time, and a stable transparent biphasic structure by a change of the density of inhomogeneities in the matrix is formed [12, 17]. The results of the FESEM and TEM are in good agreement with that of XRD and FTIRRS studies.

3.5 Dielectric constant and dielectric loss

The variation of dielectric constant (ε) and loss (tan δ) with temperature and frequency for $KNbO_3$ nano glass-ceramics, heat-treated (ceramized) at 800°C for 1 and 200 h are shown in Figs. 6(a, b) and 7(a, b), respectively. Although the dielectric measurements were carried out on seven different samples heat-treated at 800 °C for different durations between 1 to 200 h, but the data of only two samples are presented for the sake of clarity. It has been observed that room temperature dielectric constant and loss (tan δ) are virtually independent of heat-treatment time. The room temperature dielectric constant for all the samples is around 34, while loss value is 0.05. At higher temperatures the dielectric constant and the loss show an anomalous increase. This increase is further enhanced with increase in probing frequency. This anomalous increase in dielectric constant and loss at high temperature is associated with the DC conductivity of the samples due to large accumulation of K^+ ions during heat-treatment [7,18-19]. Due to high DC conductivity the cubic to tetragonal phase transition associated with potassium niobate is suppressed. However, a weak anomaly near 400°C due to cubic to

tetragonal phase transition is observed for both the samples. The dielectric permittivity shows a hump at temperatures 425° and 397°C in case of 1 and 200 h heat-treated samples respectively. This hump is very close to the phase transition temperature (420°C) of bulk $KNbO_3$ from cubic to tetragonal phase [6-8]. The variation in phase transition temperature is due to two different reasons. Firstly, the glass ceramic samples can be considered as nano-composite of $KNbO_3$ crystallites and the glass matrix. The temperature dependence of dielectric constant will show a combined effect of glass and the crystallites. Because of this combined effect the phase transition is smeared. Secondly, the size of crystallites is increasing with heat-treatment time as shown by XRD data. This leads to a different set of glass and crystallite ($KNbO_3$) matrix as the samples are heat-treated at different durations. Thus, the composite effect observed in dielectric behavior will be different in the samples heat-treated for 1 and 200 h. This will also shift the peak temperature in the dielectric behavior observed due to phase transition in $KNbO_3$ crystallites. A weak relaxation in phase transition temperature is observed in both the samples. However, this requires further investigation of dielectric behavior after removing the DC conductivity effect.

4. Conclusions

We summarize that Eu_2O_3 (0.5 wt%) doped nanometric $KNbO_3$ crystallites containing glass-ceramics have been prepared from the glass of chemical composition $25K_2O$-$25Nb_2O_5$-$50SiO_2$ (mol %) by a melt quenching technique followed by an isothermal heat-treatment at 800°C for different durations. The results on XRD, FTIRRS, FESEM, TEM and dielectric properties confirm the formation for nano-crystallite of

$KNbO_3$ in the glass matrix. The crystallite size estimated from XRD and TEM is found to be in the range of 6–12 nm. The dielectric constant and loss tangent versus temperature at different frequency revealed that the phase transition of $KNbO_3$ from cubic to tetragonal is around 425º and 397ºC (Curie temperature) for nano glass ceramic obtained from 1 and 200 h heat-treatment respectively.

Acknowledgements

This research work was supported by BRNS/DAE under the sanction No. 2007/34/05-BRNS. They gratefully thank Dr. H. S. Maiti, Director of the institute for his keen interest and kind permission to publish this work. The technical supports provided by the infrastructural facility (X-ray and Electron Microscopy Divisions) of this institute for recording XRD and TEM images are also thankfully acknowledged.

References

[1] A. Z. Simões, A. Ries, C. S. Riccardi, A. H. Gonzalez, M. A. Zaghete, B. D. Stojanovic, M. Cilense, J. A. Varela, Mater. Lett. 58 (2004) 2537.

[2] M. Zgonik, R. Schlesser, I. Biaggio, E. Voit, J. Tscherry, P. Giinter, J. Appl. Phys. 74 (1993) 1287.

[3] D. F. Xue, S. Y. Zhang, Chem. Phys. Lett. 291 (1998) 401.

[4] E. Ringgaard, T. Wurlitzer, J. Eur. Ceram. Soc. 25 (2005) 2701.

[5] Y. Li, Y. Qu, Mater. Res. Bull. 44 (2009) 82.

[6] W. P. Risk, T. R. Gosnell, A. V. Nurmikko, Compact Blue-Green Lasers, Cambridge University Press, Cambridge, 2003.

[7] S. Ding, J. Shen, J. Am. Ceram. Soc. 73 (1990) 1449.

[8] H. Birol, D. Damjanovic, N. Setter, J. Am. Ceram. Soc. 88 (2005) 1754

[9] R. S. Chaliha, K. Annapurna, A. Tarafder, V. S. Tiwari, P. K. Gupta, B. Karmakar, Solid State Sci. (2008) (Communicated).

[10] B. D. Cullity, Elements of X-Ray Diffraction, 2nd ed. Addison-Wesley Publishing Co., London, 1977.

[11] P. Pernice, A. Aronne, V. N. Sigaev, M. Kupriyanova, J. Non-Cryst. Solids 275 (2000) 216.

[12] A. Aronne, V.N. Sigaev, B. Champagnon, E. Fanelli, V. Califano, L.Z. Usmanova, P. Pernice, J. Non-Cryst. Solids 351 (2005) 3610.

[13] K. Fukumi, S. Sakka, J. Mater. Sci., 23 (1988) 2819.

[14] B. Sumuneva, St. Kralchev, V. Dimitrov, J. Non-Crys. Solids, 129 (1991) 54.

[15] J.S. deAndrade, A.G. Pinheiro, I.F. Vasconcelos, M.A.B. deArujo, M.A. Valente, A.S.B. Sombra, J. Phys. Chem. Solids 61 (2000) 899.

[16] E.N. Silva, A.P. Ayala, I. Guedes, C.W.A. Paschoal, R.L. Moreira, C.K. Loong, L.A. Boatner, Opt. Mater. 29 (2006) 224.

[17] A. Aronne, V. N. Sigaev, P. Pernice, E. Fanelli, L. Z. Usmanova, J. Non-Cryst. Solids 337 (2004) 121.

[18] D. E. Vernacotola, Key Engg. Mater. 94-95 (1994) 379.

[19] G. Shirane, H. Danner, A. Pavlovic, R. Pepinsky, Phys. Rev. 93 (1954) 672.

Figure Captions

Fig. 1. DTA curve of as-prepared glass powder.

Fig. 2. XRD patterns of as-prepared glass and those of heat-treated glasses at 800°C for 1 and 200 h.

Fig. 3. FTIRR spectra of the as-prepared (a) glass and heat-treated glasses at 800°C for (b) 1 and (c) 200 h.

Fig. 4. FESEM microphotographs of heat-treated glasses at 800°C for (a) 1 and (b) 200 h (scale bar = 100 nm).

Fig. 5. TEM images of heat-treated glasses at 800°C for (a) 1 and (b) 200 h. HRTEM images of lattice fringe of heat-treated glasses at 800°C for (c) 1 and (d) 200 h.

Fig. 6. Variation of dielectric constant (ε) as a function of temperature at different frequencies of heat-treated glasses at 800°C for (a) 1 and (b) 200 h.

Fig. 7. Variation of dielectric loss (tan δ) as a function of temperature at different frequencies of heat-treated glasses at 800°C for (a) 1 and (b) 200 h.

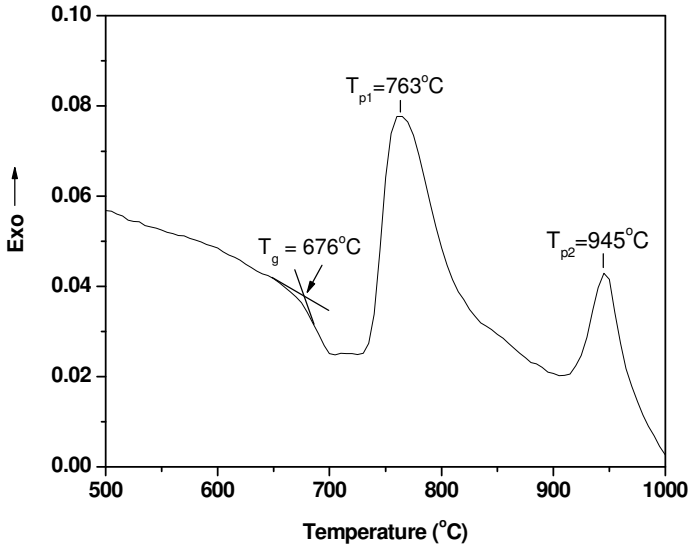
0.10
0.08
0.06
0.04
0.02
0.00
Exo
500
600
700
800
900
1000
Temperature (°C)
T_p1=763°C
T_g = 676°C
T_p2=945°C

Fig.1

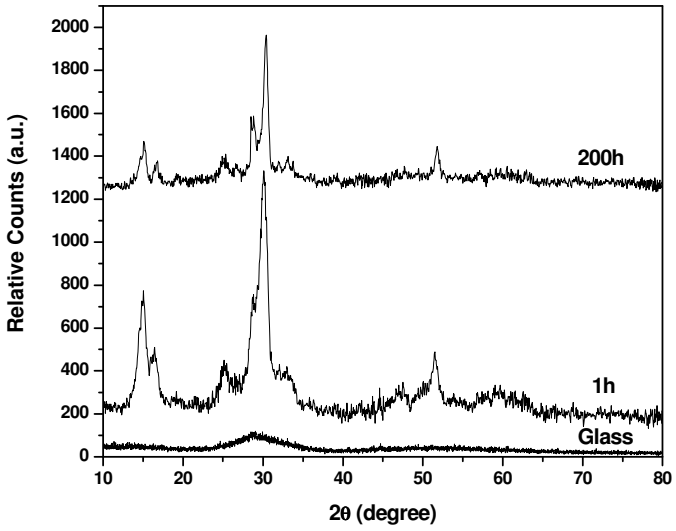
Relative Counts (a.u.)
2θ (degree)
200h
1h
Glass
0
200
400
600
800
1000
1200
1400
1600
1800
2000
10
20
30
40
50
60
70
80

Fig. 2

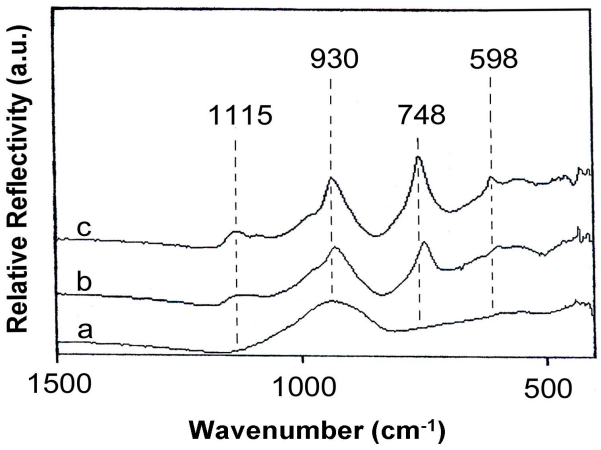
Relative Reflectivity (a.u.)
930
598
1115
748
c
b
a
1500
1000
500
Wavenumber (cm-1)

Fig. 3

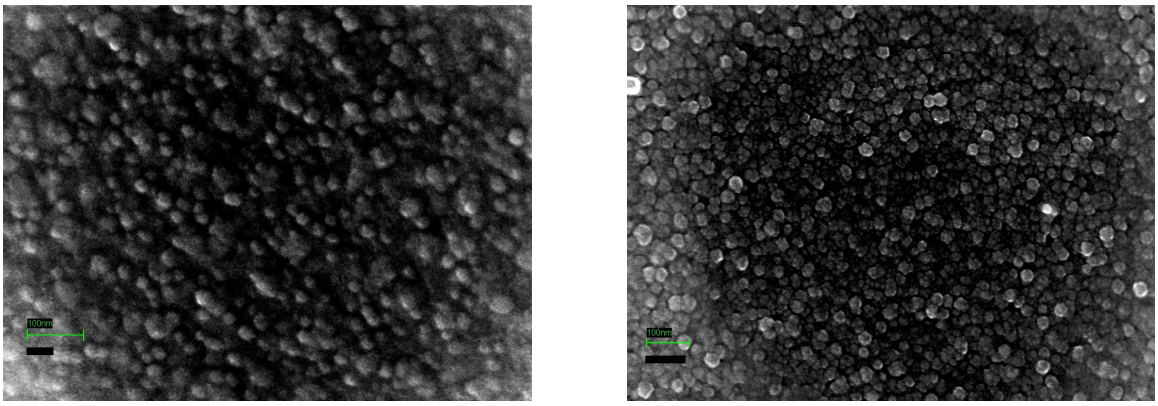

(a) (b)

Fig. 4

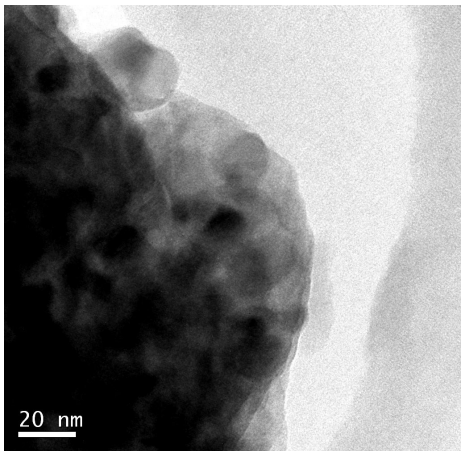

(a)

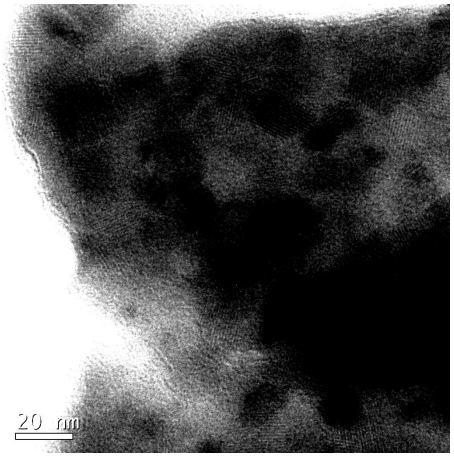

(b)

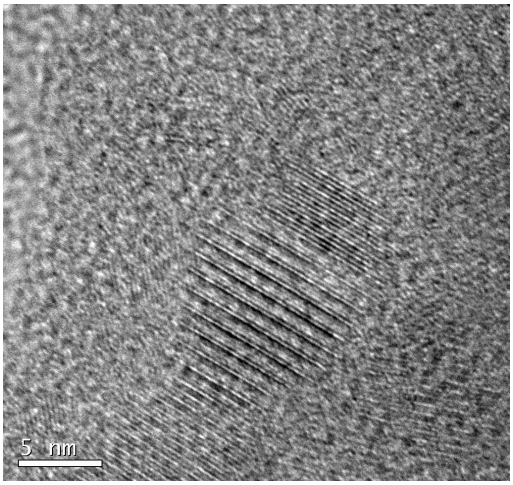

(c)

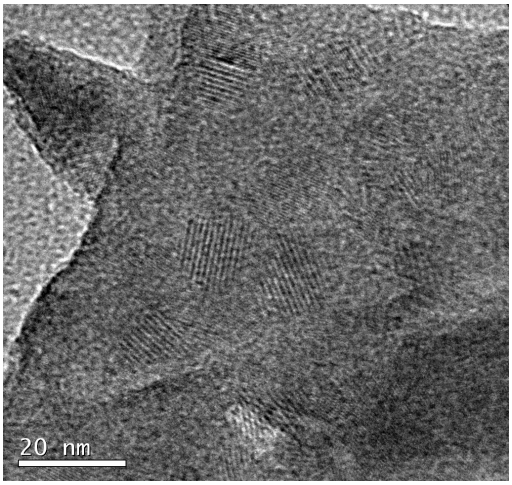

(d)

Fig. 5

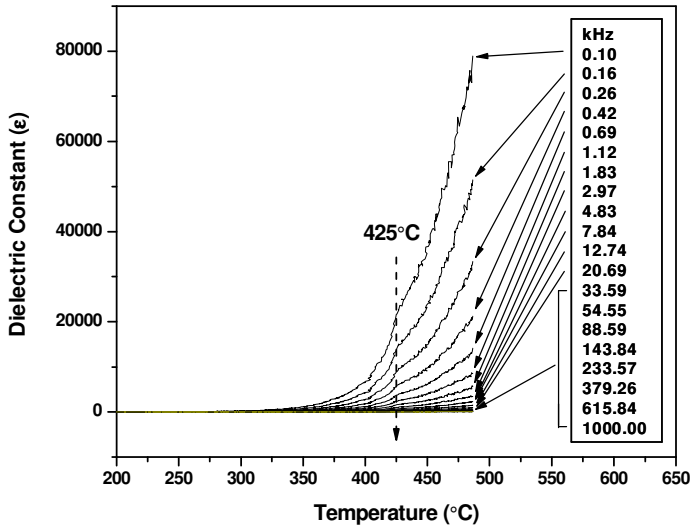
Dielectric Constant (ε)
Temperature (°C)
425°C
kHz
0.10
0.16
0.26
0.42
0.69
1.12
1.83
2.97
4.83
7.84
12.74
20.69
33.59
54.55
88.59
143.84
233.57
379.26
615.84
1000.00

(a)

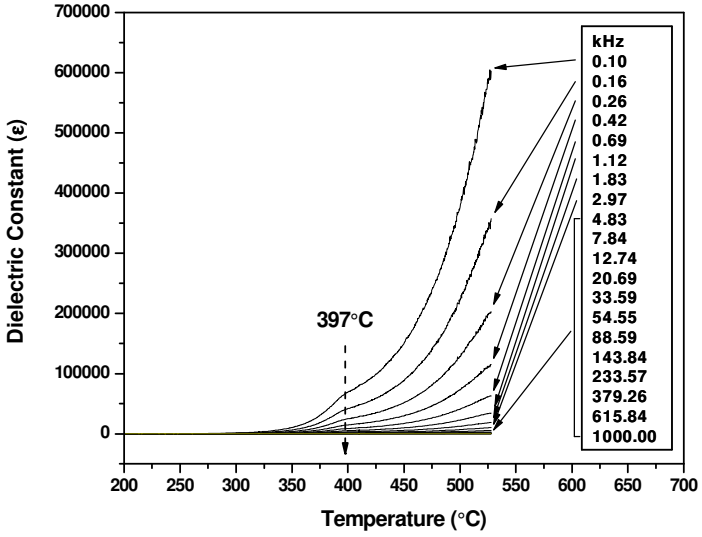
Dielectric Constant (ε)
Temperature (°C)
397°C
kHz
0.10
0.16
0.26
0.42
0.69
1.12
1.83
2.97
4.83
7.84
12.74
20.69
33.59
54.55
88.59
143.84
233.57
379.26
615.84
1000.00

(b)

Fig. 6

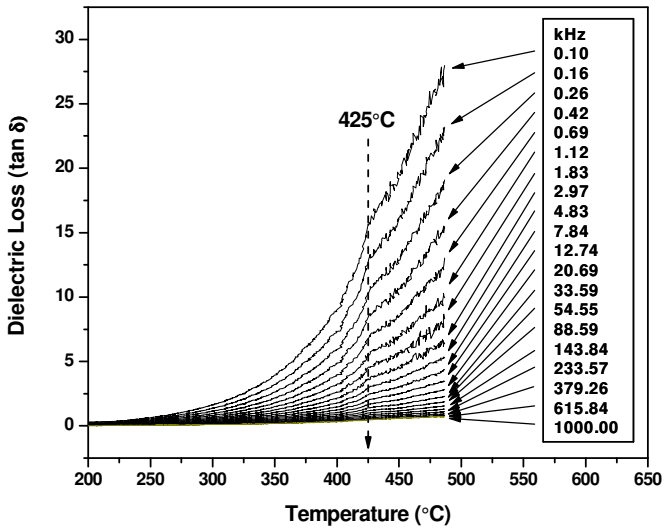
Dielectric Loss (tan δ)
Temperature (°C)
425°C
kHz
0.10
0.16
0.26
0.42
0.69
1.12
1.83
2.97
4.83
7.84
12.74
20.69
33.59
54.55
88.59
143.84
233.57
379.26
615.84
1000.00

(a)

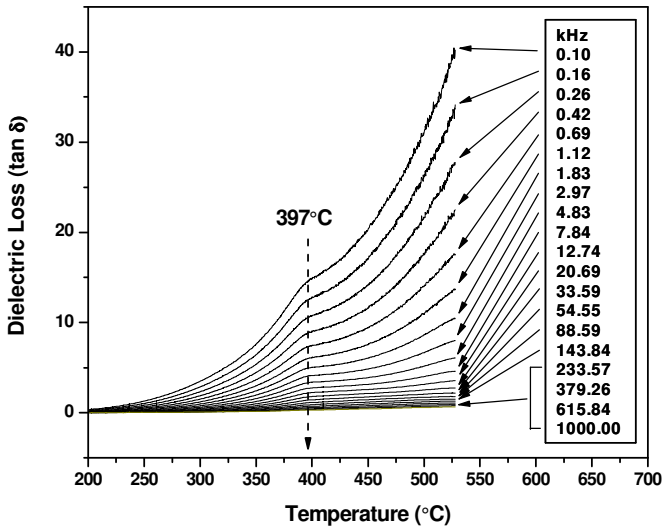
Dielectric Loss (tan δ)
Temperature (°C)
397°C
kHz
0.10
0.16
0.26
0.42
0.69
1.12
1.83
2.97
4.83
7.84
12.74
20.69
33.59
54.55
88.59
143.84
233.57
379.26
615.84
1000.00

(b)

Fig. 7